Environment International 171 (2023) 107708

Contents lists available at ScienceDirect

Environment International

journal homepage: www.elsevier.com/locate/envint

Full length article

Assessment of air quality in North Korea from satellite observations

Heesung Chong [a,1], Seoyoung Lee [a], Yeseul Cho [a], Jhoon Kim [a,*], Ja-Ho Koo [a], Yong Pyo Kim [b], Younha Kim [c], Jung-Hun Woo [d], Dha Hyun Ahn [a]

[a] Department of Atmospheric Sciences, Yonsei University, Seoul, 03722, Republic of Korea
[b] Department of Chemical Engineering and Materials Science, Ewha Womans University, Seoul, 03760, Republic of Korea
[c] International Institute for Applied Systems Analysis, A-2361, Laxenburg, Austria
[d] Department of Technology Fusion Engineering, Konkuk University, Seoul, 05029, Republic of Korea

ARTICLE INFO

Handling Editor: Xavier Querol

Keywords:
North Korea
Air quality
Satellite observations

ABSTRACT

North Korea's air quality is poorly understood due to a lack of reliable data. Here, we analyzed urban- to national-scale air quality changes in North Korea using multi-year satellite observations. Pyongyang, Nampo, Pukchang, and Munchon were identified as pollution hotspots. On a national scale, we found that North Korea experienced 6.7, 17.8, and 20.6 times greater amounts of nitrogen dioxide (NO_2), sulfur dioxide (SO_2), and carbon monoxide (CO) per unit primary energy supply (PES) than South Korea from 2005 to 2018. Besides, North Korea had a 24.3 times larger aerosol optical depth (AOD) per PES than South Korea from 2011 to 2018. Severe CO and aerosol pollution is aligned with extensive biofuel combustion. High SO_2 pollution corresponds with the strong coal dependence of the industry. The change rates of the national average columns for NO_2, SO_2, and CO were + 3.6, –4.4, and –0.4 % yr^{-1}, respectively. The AOD change rate was –4.8 % yr^{-1}. Overall decreasing trends, except for NO_2, are likely due to a decline in coal-fired PES. Positive NO_2 trends are consistent with increasing industrial activities. Each pollutant showed consistent patterns of linear trends, even after correcting the influence of transboundary pollution. Flue gas control and biofuel consumption reduction seem necessary to improve North Korea's air quality.

1. Introduction

Indoor and outdoor air pollution in the Democratic People's Republic of Korea (hereafter referred to as North Korea—NK) was responsible for 255.4 deaths per 100,000 people in 2019, the highest rate worldwide (WHO, 2022). Since NK shares borders with China and the Republic of Korea (hereafter, South Korea—SK), air quality in these countries affects one another (Bae et al., 2018; J. Choi et al., 2019; Kim et al., 2013, 2016,2019; Yeo and Kim, 2019). Inventories from 2013 and 2015 estimated that emissions in NK were 1.5 and 2.7 times those of SK for carbon monoxide (CO) and particulate matter with aerodynamic diameter $\leq$ 2.5 μm ($PM_{2.5}$), respectively (Bae et al., 2018). Considering that the primary energy supply (PES) in NK corresponded to only 3.0–3.9 % of SK's in 2013–2015, emissions of CO and $PM_{2.5}$ per unit energy supply could be tens of times larger in NK (Statistics Korea, 2019; Yeo and Kim, 2019). Moreover, NK emitted even larger amounts of nitrogen oxides (NO_x), sulfur dioxide (SO_2), and carbon dioxide (CO_2) per PES than SK in 2008, by factors of 3.9, 7.7, and 2.1, respectively (Kim and Kim, 2019). Overall, a view shared by previous studies is that NK has had a high level of air pollutant emissions per energy consumption.

Despite the severity of air pollution in NK suggested by emission inventories, observation-based assessments have been limited because the amounts of available ground-based air quality measurements are extremely small. There are very few examples of published data: international reports (e.g., UNEP, 2012) or proxy measurements such as visibility (Yeo et al., 2019). To this end, satellite data have recently been used to investigate the air quality in NK. For instance, space-borne observations of nitrogen dioxide (NO_2) enabled the estimation of NK's NO_x emissions and assessment of bottom-up inventories (Han et al., 2020; Jung et al., 2022; Kim et al., 2014; Mijling et al., 2013). Also, satellite-derived $PM_{2.5}$ concentrations allowed for analysis of the regional variability of aerosol pollution in NK (Yeo and Kim, 2019; Yeo et al., 2019). Moreover, satellite ammonia observations exposed an emission hotspot in NK (Anju city) (Van Damme et al., 2018). To date, however, satellite

* Corresponding author.
E-mail address: jkim2@yonsei.ac.kr (J. Kim).
[1] Present address: Center for Astrophysics | Harvard & Smithsonian, Cambridge, MA 02138, USA.

https://doi.org/10.1016/j.envint.2022.107708
Received 20 September 2022; Received in revised form 25 November 2022; Accepted 19 December 2022
Available online 20 December 2022

products have been employed only within the context of a single pollutant to characterize NK's air quality. A comprehensive air quality assessment using satellite observations is hardly found, except NK was briefly mentioned while covering a broader area in East Asia (e.g., Qu et al., 2022). To better understand the air quality in NK and develop mitigation measures, it is necessary to analyze trends of multiple species in accordance with changes in energy consumption (Kim and Kim, 2019).

The present study aimed to assess urban- to national-scale air quality in NK using multiple satellite observations for the first time. Pollutants of interest were NO_2, SO_2, CO, and aerosols, whose amounts are strongly associated with anthropogenic activities. Tropospheric NO_2 is produced predominantly via fossil fuel combustion, and to a lesser degree, by biomass burning, soil emissions, and lightning (Conrad, 1996; Ridley et al., 1996; Van Vuuren et al., 2011). Atmospheric SO_2 levels are also largely derived from anthropogenic sources, including fossil fuel combustion, smelters, and oil refineries (Fioletov et al., 2016; Smith et al., 2011). CO originates predominantly from biomass burning and the incomplete combustion of fossil fuels during industrial activities, vehicle use, and domestic heating (Zhong et al., 2017). Ambient aerosols, the key contributor to various adverse effects of pollution on human health (Apte et al., 2015; Wu et al., 2018), are either emitted directly from anthropogenic and natural sources or produced during chemical reactions of their precursors (e.g., NO_2, SO_2, and ammonia).

Satellite observations of all these pollutants have accumulated over North Korea for multiple years or even decades, allowing for long-term trend analysis. Besides, recently proposed oversampling methods facilitated the space-borne detection of urban-scale pollution (Pommier et al., 2013; Sun et al., 2018; Zhu et al., 2017). Exploiting these advances, we explored pollution hotspots in NK and analyzed trends for 2005–2018 by oversampling NO_2 and SO_2 columns from the Ozone Monitoring Instrument (OMI) and CO columns from the Measurements of Pollution in the Troposphere (MOPITT). For aerosol pollution investigation, we used 6 km resolution datasets of aerosol optical depth (AOD) for 2011–2018 and $PM_{2.5}$ concentrations for 2015–2018 from the Geostationary Ocean Color Imager (GOCI). After characterizing the spatiotemporal variability of air pollution in NK, we suggest possible contributors to the air quality changes based on previous studies and official national statistics for NK.

To put the severity of NK's air pollution into perspective, this study compared statistics between NK and SK, including pollutant amounts and PES. The areas of interest for SK were (1) the entirety of SK territory and (2) Seoul, the capital. Satellite datasets were sampled using the same methods for NK and SK. By aggregating the comparison results between NK and SK for all pollutants of interest, we comprehensively assess NK's air quality.

2. Materials and methods

2.1. Satellite data

2.1.1. OMI NASA NO_2 and SO_2 products

The OMI instrument is a nadir-viewing ultraviolet (UV)–visible (VIS) spectrometer launched in 2004 onboard the Aura satellite (Levelt et al., 2006). OMI has 60 cross-track fields of view (FOVs), with spatial resolutions of ~ 13 km × 24 km at nadir and ~ 28 km × 150 km at the swath edges. The overpass time of OMI is 13:30–14:00 local time (LT), and its ~ 2600 km wide swath typically provides 1–2 overpasses per day across the Korean Peninsula. Examples of OMI observations over NK can also be found in previous studies targeting a broad domain in East Asia (Han et al., 2011; Han, 2020; Lee et al., 2014; Souri et al., 2017). Here, OMI data were acquired from January 2005 to December 2018. We excluded OMI observations affected by the so-called "row anomaly," characterized by abnormally low radiance readings found in certain cross-track FOVs since 2007 (Schenkeveld et al., 2017).

To assess the changes in vertical column densities (VCDs) of NO_2 over NK, we employed the NASA OMI NO_2 standard product (OMNO2) (Krotkov et al., 2019a). Recent validation studies found high correlations in East Asia by comparing the OMNO2 product with ground-based in-situ measurements ($r = 0.78$, Cai et al., 2022) and multi-axis differential optical absorption spectroscopy (MAX-DOAS) observations ($r = 0.88$, Cheng et al., 2019). We employed the most recent version (4.0) of the product for analyses (Lamsal et al., 2021). Tropospheric VCD (TVCD) data were used for analyzing anthropogenic NO_2 pollution. Only those observations with cloud radiance fractions < 0.3, solar zenith angles $< 70°$, and good data quality (as stated by the quality flags, 'VcdQualityFlags' $= 0$) were used here (Krotkov et al., 2019b).

We investigated spatiotemporal variations in SO_2 VCDs over NK using planetary boundary layer (PBL) data from the NASA OMI SO_2 product (OMSO2), which were derived using principal component analysis (PCA) (Krotkov et al., 2020; Li et al., 2020a). Long-term validation of the OMSO2 product in East Asia showed good agreements with ground-based in-situ measurements ($r = 0.62$, Si et al., 2019) and MAX-DOAS observations ($r^2 = 0.54$, Tian et al., 2018). We used the latest version of the product in this study (version 2; Li et al., 2020b). As recommended by the data source, the variable ColumnAmountSO2 was used for the analyses related to anthropogenic SO_2 pollution. SO_2 observations from rows 4 to 54 (zero-based) of the OMI charge-coupled device (CCD) detector were used here, except for those from the descending node of the Aura satellite. Observations with radiative cloud fractions > 0.3, solar zenith angles $> 65°$, and AMFs < 0.3 were excluded, along with the SO_2 VCDs from pixels with snow or ice. To focus on anthropogenically-driven SO_2 concentrations, we masked transient volcanic SO_2 clouds by excluding OMI swaths, whose 99.9 percentile of SO_2 VCDs within 123–131°E, 33–43°N exceeded 9.5 DU, adopting the approach of Krotkov et al. (2016). This approach removed 8 swaths, corresponding to < 1 % of those used in the present study.

2.1.2. MOPITT CO product

MOPITT was launched in December 1999 onboard the NASA Terra satellite, with local equator crossing times of ~ 10:30 and ~ 22:30 (Edwards et al., 2004). MOPITT observations over NK can also be found in previous studies analyzing CO emissions and trends in East Asia (e.g., Zheng et al., 2018). For CO analyses in this study, Level-2 data were used from the MOPITT-derived CO (NIR and thermal IR radiances) V008 product (MOP02J_8), providing vertical profiles of volume mixing ratios (VMRs) and total VCDs at 22 km × 22 km horizontal resolution (MOPITT Algorithm Development Team, 2018; NASA/LARC/SD/ASDC, 2000). This study employed the total VCD values instead of surface VMRs, to account for different injection heights of CO into the air (Kim et al., 2019). Validation of total CO VCDs from this product over the Korean Peninsula showed a bias of -1.80×10^{16} molecules cm^{-2} and a standard deviation of 2.23×10^{17} molecules cm^{-2} (Deeter et al., 2022), which are 1–2 orders of magnitude smaller than typical CO VCDs in NK (see Fig. 2f). All pixels with solar zenith angles of $> 80°$ were excluded in this study.

2.1.3. GOCI AOD product

The GOCI instrument was launched onboard the Communication, Ocean, and Meteorological Satellites (COMS) in 2010 as the first ocean color imager operating from a geostationary orbit (Choi et al., 2012). GOCI measured hourly backscattered sunlight from 00:30 to 07:30 UTC at a 500 m resolution within a 2,500 km × 2,500 km domain centered at 36°N and 130°E. Aerosol optical properties (AOPs) retrieved from GOCI at 6 km resolution by the Yonsei aerosol retrieval (YAER) algorithm showed comparable accuracy to that of ground-based and other satellite-based observations (M. Choi et al., 2016, 2018; M. Choi et al., 2019; Lee et al., 2010). The GOCI YAER version 2 product was used here, which has previously been effectively employed for assessing air quality across the Korean Peninsula (Lee et al., 2019, 2021). This study used the GOCI AOD product from March 2011 (the earliest month available) to December 2018. GOCI AODs at 550 nm showed an excellent agreement

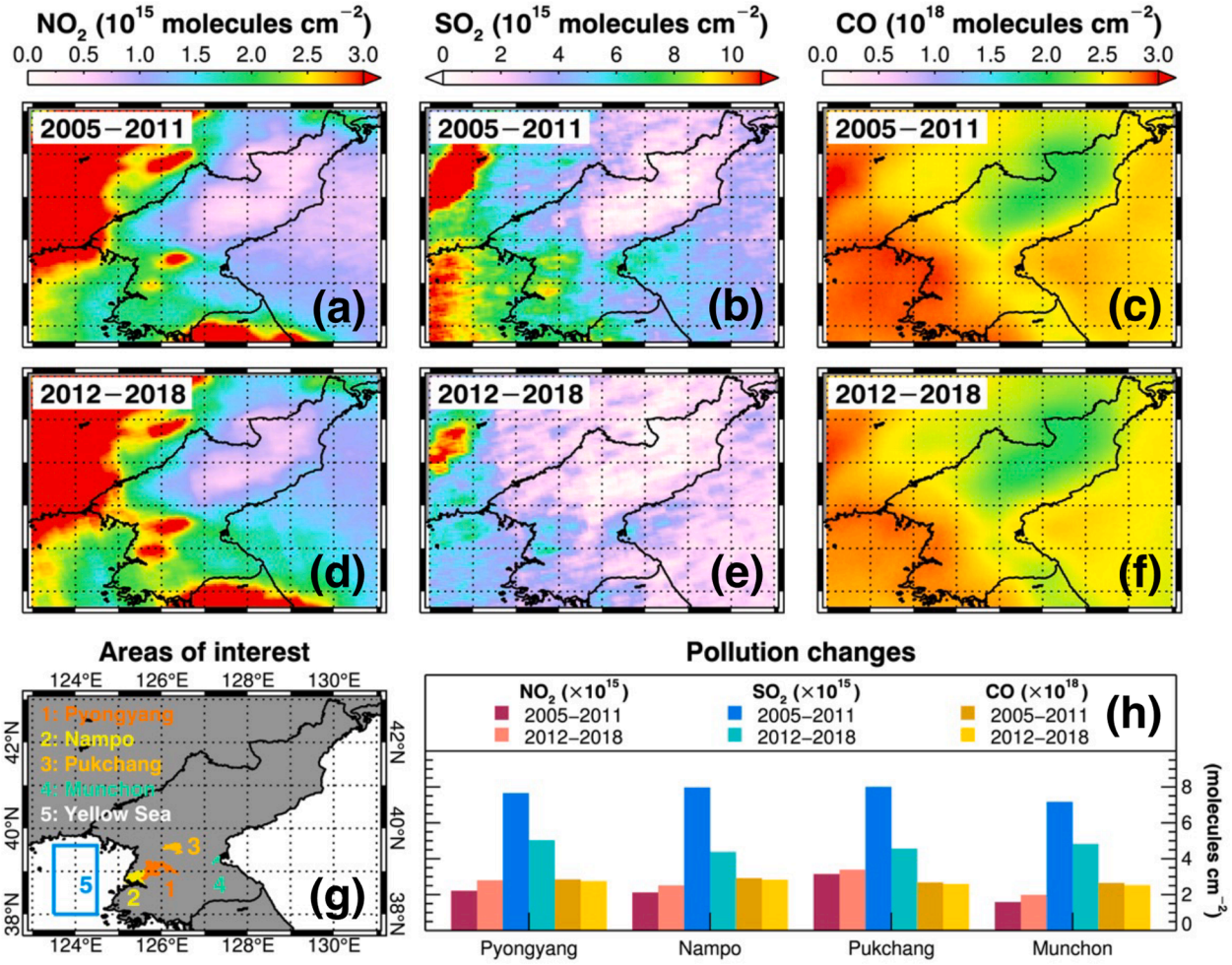

Fig. 1. Changes in NO_2 TVCDs, SO_2 VCDs, and CO VCDs across North Korea. Panels (a–c) indicate the averages for 2005–2011, and panels (d–f) represent those for 2012–2018. Panel (g) shows the cities of interest: Pyongyang, Nampo, Pukchang, and Munchon, in addition to the reference sector (123.5–124.5°E, 38.0–39.6°N) over the Yellow Sea. Panel (h) shows NO_2, SO_2, and CO VCD values averaged for 2005–2011 and 2012–2018 in the selected cities. (For interpretation of the references to color in this figure legend, the reader is referred to the web version of this article.)

with ground-based observations from the Aerosol Robotic Network (AERONET) (r = 0.92) from March 2011 to February 2016 over land (Choi et al., 2018). The observed wavelength of AOD is omitted hereafter, as only 550 nm was assessed in this study.

2.2. Methods

2.2.1. Estimating surface $PM_{2.5}$ concentrations

Surface $PM_{2.5}$ concentrations were estimated using the random forest (RF; Breiman, 2001) algorithm at a native GOCI AOP resolution of 6 km. We constructed the RF model using GOCI AOP products, meteorological and land variables, ancillary data, and ground-based $PM_{2.5}$ measurements. The GOCI AOP products included AOD, fine mode fraction at 550 nm, and surface reflectance at 660 nm. The meteorological variables were from the European Center for Medium-Range Weather Forecast (ECMWF) reanalysis data (ERA5; Hersbach et al., 2020) and comprised temperature, pressure, wind speed, boundary layer height, and relative humidity (RH). The RH was calculated using atmospheric and dew point temperatures at the surface by applying the August–Roche–Magnus formula. For the land variables, low and high vegetation covers were used. Following previous studies, the cosine (Feng et al., 2015) and sine (Park et al., 2019) of the day of the year were employed as ancillary data. The spatial domain of the $PM_{2.5}$ estimates was 118–132°E, 32–44°N. For hourly surface $PM_{2.5}$ information, Airkorea data (https://www.airkorea.or.kr/eng) were employed for SK, the China National Urban Air Quality Real-time Publishing Platform data (https://106.37.208.233:20035/) for China, and the Ministry of the Environment (https://www.nies.go.jp/igreen/) with the Atmospheric Environmental Regional Observation System (AEROS) data (https://soramame.taiki.go.jp) for Japan.

The probability distributions of $PM_{2.5}$ concentrations are typically skewed low; thus, low values are more frequently sampled while constructing the training set for RF, which can lead to the underestimation of satellite-derived values. To address this issue, we oversampled high $PM_{2.5}$ concentrations in training by applying the synthetic minority oversampling technique (SMOTE) (Chawla et al., 2002).

$PM_{2.5}$ concentrations were estimated on an annual basis, and results were evaluated using a 10-fold cross-validation approach (Rodríguez et al., 2010). The estimates only cover 2015–2018, as official data of ground-based $PM_{2.5}$ concentration in SK have existed since 2015. The corresponding annual coefficients of determination (R^2) for 2015–2018 were 0.714, 0.699, 0.690, and 0.683, respectively. The validation results and the mean $PM_{2.5}$ concentrations over NK for the entire 4-year period are shown in Fig. S1.

2.2.2. Oversampling satellite observations

To generate high-resolution gridded data for OMI NO_2 and SO_2 VCDs, we applied an oversampling approach known as the tessellation method. This approach assumes each OMI FOV to be a quadrilateral on the earth's surface and calculates an area- and error-weighted average

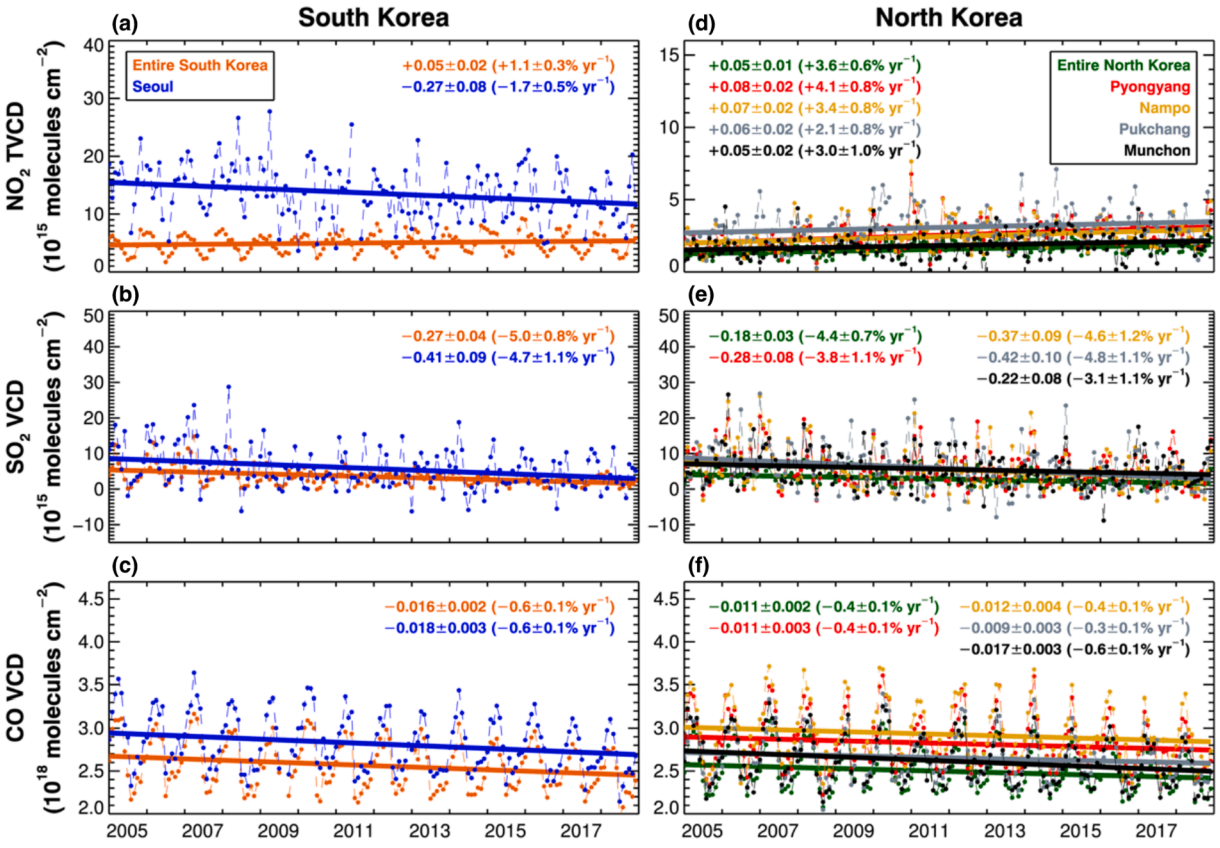

Fig. 2. Time series of NO_2 TVCDs, SO_2 VCDs, and CO VCDs in South and North Korea from 2005 to 2018. Colors correspond to different regions. Thin, dashed lines indicate monthly data, and thick lines represent linear regression fits. Inset values represent the absolute (relative) trends. Absolute trends are in 10^{15}, 10^{15}, and 10^{18} molecules cm^{-2} yr^{-1} for NO_2, SO_2, and CO, respectively. Note that panels (a) and (d) have different y-axis ranges.

VCD for each grid cell (Eq. (1)):

$$\overline{C}(j) = \frac{\sum_i \frac{A(i,j)}{S(i)\sigma(i)} C(i)}{\sum_i \frac{A(i,j)}{S(i)\sigma(i)}}, \quad (1)$$

where $C(i)$ is an OMI VCD at FOV i, $\sigma(i)$ represents its precision, $S(i)$ is the area of FOV i, $A(i,j)$ denotes the overlapping area between FOV i and grid cell j, and $\overline{C}(j)$ is the resultant average VCD at grid cell j. More detailed descriptions of this oversampling method can be found in the studies of Zhu et al. (2017) and Sun et al. (2018). The longitudes and latitudes of the four corners of an OMI FOV were defined by the OMI pixel corner product (OMPIXCOR version 3) (Kurosu and Celarier, 2010). Tessellation was performed on 0.05° × 0.05° grid cells for both OMNO2 and OMSO2 products. For the OMSO2 product, unity was input for $\sigma(i)$ in Eq. (1) as pixel-level precision was not provided.

The MOPITT datasets did not include the pixel corner (vertex) information in the variable list; therefore, an approach known as "pixel averaging" (Fioletov et al., 2011) or "point oversampling" (Sun et al., 2018) was applied to oversample CO VCDs (Pommier et al., 2013). This approach produces gridded data by averaging the CO VCDs from pixels located within a particular radius from each grid. The present study employed a 28 km radius to oversample MOPITT CO VCDs onto 0.05° × 0.05° grids.

As the 6 km spatial resolution of GOCI AOD data is adequate for urban/regional-scale air quality analysis (Choi et al., 2018), this data was employed without oversampling.

2.2.3. Time series analysis

This study assumed that the time series of monthly satellite observations at each grid was composed of three subcomponents (Eq. (2)) (Bhardwaj et al., 2019; Weatherhead et al., 1998):

$$\overline{C}(t) = \alpha(t) + \beta \times \frac{t}{12} + \varepsilon(t), \quad (2)$$

where t represents time (month), $\alpha(t)$ is a seasonal component, β is a linear annual trend component, and $\varepsilon(t)$ is a residual component. Here, the α term was derived by combining a constant and sinusoidal harmonic series:

$$\alpha(t) = \gamma_0 + \sum_{k=1}^{3}\left(\gamma_{1k}\sin\left(\frac{2\pi kt}{12}\right) + \gamma_{2k}\cos\left(\frac{2\pi kt}{12}\right)\right), \quad (3)$$

where γ_0, γ_{1k}, and γ_{2k} are constant coefficients. The removal of the second term (the sine and cosine terms combined) on the right-hand side of Eq. (3) is referred to as "deseasonalization" in this study. The uncertainty of the linear trend σ_β is estimated according to Eq. (4) (Weatherhead et al., 1998):

$$\sigma_\beta = \frac{\sigma_\varepsilon}{l^{3/2}}\sqrt{\frac{1+\delta}{1-\delta}}, \quad (4)$$

where σ_ε is the standard deviation of the residuals ε(t), l is the number of years, and δ is the autocorrelation coefficient of $\varepsilon(t)$ calculated with a 1-month lag. If the ratio $|\beta/\sigma_\beta| \geq 2$, the trend β is significant at the 95 % confidence level.

3. Results and discussion

3.1. Changes in atmospheric NO_2, SO_2, and CO pollution from 2005 to 2018

Comparisons of average pollution levels between 2005–2011 and

2012–2018 indicated that over the entire NK territory, TVCDs of NO_2 increased, while total VCDs of SO_2 and CO decreased (Fig. 1). Oversampling satellite observations onto 0.05° × 0.05° grids enabled the detection of pollution hotspots, particularly for NO_2 and SO_2, which have shorter lifetimes than CO. The VCDs of these three gaseous species showed overlapping high values in the western region, an area of high population density and low terrain elevations (Fig. S2) that is affected by transboundary pollution (Fig. S3). Pyongyang, Nampo, Pukchang, and Munchon were selected as the cities of interest for the analyses due to their elevated NO_2, SO_2, and CO VCDs (Fig. 1).

Relatively large NO_2 and CO VCDs in the capital Pyongyang can be partly attributed to vehicular emissions, as this is the most populated region in NK (Fig. S2a). Also, Pyongyang has the largest industrial district in NK, which comprises thermal power plants, steel mills, and machine plants (Dormels, 2014), contributing to the high NO_2 and SO_2 VCD values. Nampo is a port city and a national hub of the shipbuilding and smelting industries; thus, its large VCDs of NO_2, SO_2, and CO are likely associated with industrial emissions, including shipyards and steel mills (Dormels, 2014). The Pukchang Thermal Power Plant, the most substantial thermal power plant in NK (Dormels, 2014; Yeo and Kim, 2018), presumably contribute to the large local NO_2 and SO_2 VCDs in Pukchang. The city of Munchon belongs to the Wonsan industrial district along the eastern coastal area of NK (Dormels, 2014); thus, the high local NO_2 and SO_2 VCD values are likely caused by smelters and other industrial-facility emissions. The relative changes in average NO_2 TVCDs from 2005–2011 to 2012–2018 were + 26, +19, +8, and + 25 % for Pyongyang, Nampo, Pukchang, and Munchon, respectively, all of which indicated NO_2 increases. Meanwhile, SO_2 VCD changes corresponded to –34, –45, –43, and –33 %, respectively, and total CO VCDs decreased by 3–4 % in all four cities. We also found consistent hotspots and percentage changes for NO_2 and SO_2 VCDs by applying the "physical oversampling" method (Sun et al., 2018) (see Supplementary data), even though it resulted in lower values of 7-year mean VCDs than tessellation in four selected cities (Figs. S4 and S5). This consistency corroborates the air pollution changes in NK discussed above.

Further assessments of NK's air quality presented below were performed by constructing monthly mean VCD datasets. Satellite observations were oversampled every month using the tessellation method, and linear trends were calculated for the entire 14-year period (Fig. 2). Calculation results are listed in Table 1, along with the 14-year average VCDs. Negative monthly SO_2 VCDs were derived when the averaged data point number was insufficient to smooth out negative daily VCDs that were possibly generated by SO_2 concentrations below the OMI detection limit (Fig. 2). Such negative VCDs were not excluded from the trend estimation for their implication for low SO_2 concentrations.

The NO_2 TVCD averaged for the entire NK territory for 2005–2018 was 31 % of that observed in SK (Table 1). Among the cities examined in NK, Pukchang showed the largest mean NO_2 TVCD, likely due to the emissions from the Pukchang Thermal Power Plant. The relative linear trends of NO_2 TVCDs over the selected four cities in NK ranged between + 2.1–4.1 % yr^{-1}, and rates over the entire territory showed a similar positive trend of + 3.6 ± 0.6 % yr^{-1} (Fig. 2d). To put the severity of NO_2 pollution into perspective, we compared TVCDs between NK and SK in association with their respective PES values (Table 1). From 2005 to

Table 1
Mean values and trends of NO_2 TVCD, SO_2 VCD, CO VCD, AOD, $PM_{2.5}$ concentrations, and primary energy supply (PES) over South and North Korea. The PES values are in a unit of ton of oil equivalent (TOE). The Yellow Sea in the bottom row represents the reference sector at 123.5–124.5°E, 38.0–39.6°N (see Fig. 1g).

			NO_2	SO_2	CO	AOD	$PM_{2.5}$	PES
Period			*2005–2018*			*March 2011– December 2018*	*2015–2018*	*2005–2018*
Unit		Mean Linear trend	10^{15} molecules cm^{-2} 10^{15} molecules cm^{-2} yr^{-1}		10^{18} molecules cm^{-2} 10^{18} molecules cm^{-2} yr^{-1}	(dimensionless) yr^{-1}	μg m^{-3} μg m^{-3} yr^{-1}	10^3 TOE 10^3 TOE yr^{-1}
South Korea	*Entire nation*	Mean	5.01 ± 1.67	3.51 ± 2.65	2.57 ± 0.28	0.28 ± 0.12	27.5 ± 5.3	268,319 ± 26,681
		Linear trend (in %)	+0.05 ± 0.02 (1.1 ± 0.3)	–0.27 ± 0.04 (–5.0 ± 0.8)	–0.02 ± 0.002 (–0.6 ± 0.1)	–0.018 ± 0.005 (–5.1 ± 1.3)	–1.4 ± 0.3 (–4.7 ± 0.7)	6,250 ± 368 (2.7 ± 0.2)
	Seoul	Mean	13.72 ± 4.59	5.82 ± 5.80	2.82 ± 0.32	0.33 ± 0.16	25.5 ± 6.6	–
		Linear trend (in %)	–0.27 ± 0.08 (–1.7 ± 0.5)	–0.41 ± 0.09 (–4.7 ± 1.1)	–0.02 ± 0.003 (–0.6 ± 0.1)	–0.019 ± 0.006 (–4.6 ± 1.4)	–1.0 ± 0.6 (–3.8 ± 1.7)	–
North Korea	*Entire nation*	Mean	1.57 ± 0.45	2.84 ± 1.99	2.50 ± 0.24	0.26 ± 0.11	41.8 ± 12.0	13,562 ± 3,013
		Linear trend (in %)	+0.05 ± 0.01 (3.6 ± 0.6)	–0.18 ± 0.03 (–4.4 ± 0.7)	–0.011 ± 0.002 (–0.4 ± 0.1)	–0.015 ± 0.003 (–4.8 ± 1.0)	–0.3 ± 0.5 (–0.6 ± 1.2)	–572 ± 126 (–3.3 ± 0.7)
	Pyongyang	Mean	2.55 ± 0.88	5.59 ± 5.04	2.83 ± 0.31	0.31 ± 0.14	49.6 ± 13.7	–
		Linear trend (in %)	+0.08 ± 0.02 (4.1 ± 0.8)	–0.28 ± 0.08 (–3.8 ± 1.1)	–0.011 ± 0.003 (–0.4 ± 0.1)	–0.018 ± 0.005 (–4.6 ± 1.2)	–3.3 ± 1.2 (–5.9 ± 2.1)	–
	Nampo	Mean	2.46 ± 1.00	5.51 ± 5.52	2.93 ± 0.34	0.36 ± 0.16	46.4 ± 11.5	–
		Linear trend (in %)	+0.07 ± 0.02 (3.4 ± 0.8)	–0.37 ± 0.09 (–4.6 ± 1.2)	–0.012 ± 0.004 (–0.4 ± 0.1)	–0.014 ± 0.006 (–3.4 ± 1.4)	–2.8 ± 0.8 (–5.3 ± 1.5)	–
	Pukchang	Mean	3.11 ± 1.13	5.84 ± 6.09	2.66 ± 0.27	0.24 ± 0.14	46.7 ± 18.7	–
		Linear trend (in %)	+0.06 ± 0.02 (2.1 ± 0.8)	–0.42 ± 0.10 (–4.8 ± 1.1)	–0.009 ± 0.003 (–0.3 ± 0.1)	–0.015 ± 0.004 (–5.3 ± 1.5)	–1.8 ± 1.4 (–3.4 ± 2.7)	–
	Munchon	Mean	1.84 ± 0.86	5.59 ± 4.98	2.62 ± 0.29	0.26 ± 0.14	38.1 ± 14.0	–
		Linear trend (in %)	+0.05 ± 0.02 (3.0 ± 1.0)	–0.22 ± 0.08 (–3.1 ± 1.1)	–0.017 ± 0.003 (–0.6 ± 0.1)	–0.020 ± 0.004 (–5.9 ± 1.1)	0.2 ± 1.2 (–0.6 ± 3.2)	–
Yellow Sea		Mean	2.64 ± 1.24	6.12 ± 4.80	2.96 ± 0.37	0.29 ± 0.12	31.5 ± 7.1	–
		Linear trend (in %)	+0.04 ± 0.02 (1.7 ± 0.8)	–0.49 ± 0.08 (–5.1 ± 0.9)	–0.014 ± 0.004 (–0.5 ± 0.1)	–0.014 ± 0.004 (–4.0 ± 1.0)	–1.2 ± 0.5 (–3.6 ± 1.4)	–

2018, the PES in NK declined by 3.3 ± 0.7 % yr^{-1}, whereas SK's PES increased by 2.7 ± 0.2 % yr^{-1}; however, the relative increase in NO_2 TVCDs was faster in NK (+3.6 ± 0.6 % yr^{-1}) than in SK (+1.1 ± 0.3 % yr^{-1}) (Fig. 2a and d). Considering that anthropogenic NO_2 emissions are most commonly a consequence of energy consumption, it is exceptional that the NO_2 TVCD increased in NK as PES decreased. Dividing the national average NO_2 TVCDs by the annual PES, levels in NK were greater than those of SK by an average factor of 6.7, with an increasing trend (11.9 % yr^{-1}). The large values of NO_2 TVCD per PES indicate that the air quality in NK has been poorly controlled, suffering from low removal efficiencies and high emission coefficients.

The average SO_2 VCD in NK for 2005–2018 corresponded to 81 % of that recorded in SK over the same period (Table 1). The SO_2 VCD ratio of NK to SK was significantly higher than NO_2, likely due to extensive coal burning in NK. The International Energy Agency (IEA) reported that coal-fired energy generally accounts for 60–80 % of PES in NK (IEA, 2022). The largest mean SO_2 VCD among the four NK cities appeared in Pukchang, likely resulting from a combination of power plant emissions and transboundary pollution. Contrary to NO_2 TVCDs, SO_2 VCDs showed negative trends over all cities analyzed in NK (Fig. 2e). The national average SO_2 VCDs for NK also showed a negative trend of –4.4 ± 0.7 % yr^{-1}; however, SO_2 VCDs per unit PES were still larger in NK than in SK. The average ratio of SO_2 VCD per unit PES between NK and SK was 17.8 from 2005 to 2018 (even higher than NO_2). Severe SO_2 pollution in NK is possibly due to the lack of desulfurization of fuels and flue gases.

The average CO VCD ratio between NK and SK was 97 %, the largest among the gaseous species of interest (Table 1). On average, NK experienced a 20.6 times larger CO VCD per unit PES than SK from 2005 to 2018. The most severe CO pollution in NK was recorded in Nampo. The large CO VCDs in NK can be attributed to transboundary pollution and domestic emissions from coal and biofuel combustion. The pollution levels declined from 2005 to 2018, but the rates were slow; the CO VCDs decreased over the four selected cities and the entirety of NK at rates between –0.6 and –0.3 % yr^{-1} (Fig. 2f). The CO VCDs slowly decreased by 0.5 ± 0.1 % yr^{-1} also over the reference sector in the Yellow Sea (see Fig. 1g for the definition of the reference sector), implying the continuous effects of long-range transport from China on CO pollution over NK (Table 1; Fig. S6c). Domestically, previous studies found that residential biomass burning was responsible for a significant proportion of CO emissions in NK (Kim et al., 2011; Kim and Kim, 2019), although

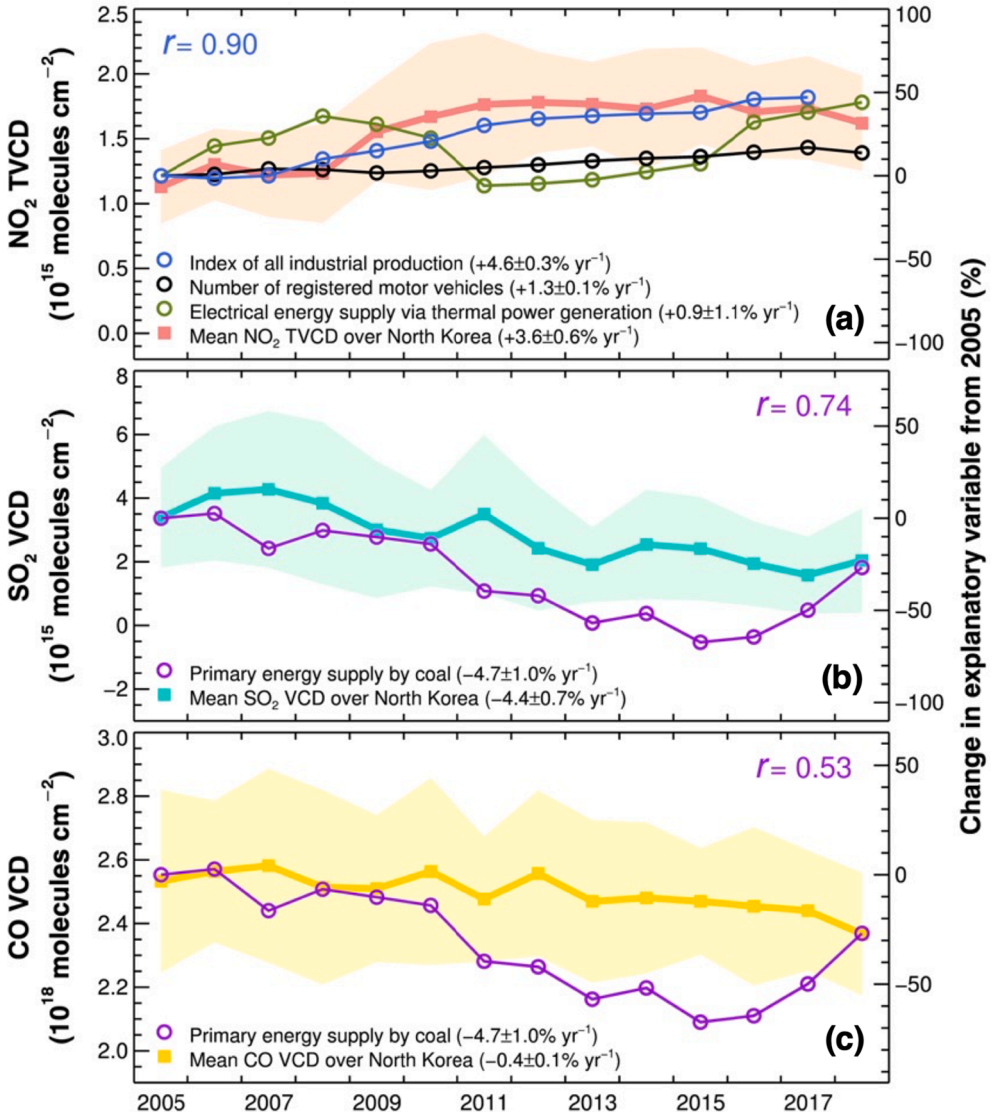

Fig. 3. Time series of annual mean (a) NO_2 TVCDs, (b) SO_2 VCDs, and (c) CO VCDs across North Korea. Changes in explanatory variables are overlaid. Shading indicates standard deviations of the VCDs across North Korea. Insets present the relative trend values and correlation coefficients between the VCDs and explanatory variables. For NO_2, the correlation coefficient was calculated using the index of all industrial production.

estimates of local biofuel consumption vary greatly by data sources (IEA, 2022; Streets et al., 2003; UNEP, 2012). For example, Streets et al. (2003) estimated that up to 40 % of NK's CO emissions originated from biofuel combustion in 2000.

According to the major statistical indicators published by the SK's government (Statistics Korea, 2018, 2019), coal-fired PES in NK decreased during 2005–2018 at a rate of –4.7 % yr^{-1} (Fig. 3b and c). Considering the strong coal dependence of NK's industry (Kim and Kim, 2019; Yeo and Kim, 2019), one may expect that local NO_2 and SO_2 VCDs would display similar decreasing patterns across the study period. Indeed, SO_2 VCDs decreased, but NO_2 TVCDs showed positive trends (Fig. 3a and b). Mijling et al. (2013) and Lee et al. (2014) suggested that transboundary pollution from China affected NK's NO_2 pollution. To examine pollution changes in NK driven only by domestic factors, we attempted to correct the influence of transboundary pollution by removing the dependency of NO_2 TVCDs in NK on those observed in the reference sector in the Yellow Sea (see Supplementary data). This reference sector was selected for two reasons: (1) it has minimal local emissions (generally restricted to those from ships), and (2) air masses from China typically travel to this region before arriving at the Korean Peninsula (Bhardwaj et al., 2019; Lee et al., 2021) (see Fig. S7). However, the positive NO_2 trends were preserved even after correcting for the effects of transboundary pollution (Figs. S6d and S8a).

Moreover, seasonal mean NO_2 TVCDs revealed several features implying that domestic factors maintained a significant influence on the positive trends separately from the transboundary pollution (Fig. S9). First, NK's NO_2 TVCDs in spring (MAM) indicated a positive trend of 3.7 $\times$ 10^{13} molecules cm^{-2} yr^{-1}, significantly larger than the spring trend over the Yellow Sea (0.8 $\times$ 10^{13} molecules cm^{-2} yr^{-1}). Second, the maximum positive trend in NK appeared in autumn (SON), while the most rapid increase over the Yellow Sea was observed in winter (DJF). Third, the NO_2 TVCDs in NK increased more rapidly than over the Yellow Sea in summer (JJA). Fourth, NO_2 TVCDs in NK were generally the largest in spring (MAM), while maximum values over the Yellow Sea were typically seen in winter (DJF).

We examined if soil emissions were significant factors in the increasing NO_2 trends in NK, based on a previous study suggesting that NO_2 TVCDs typically peaked in summer in regions where soil emissions dominated (van der A et al., 2008). Seasonal analysis of the maximum NO_2 TVCD at each grid pixel in NK showed that TVCDs increased more rapidly at grids where maximum TVCDs were observed outside of the summer season (Fig. S10). Furthermore, grids with maximum NO_2 values in JJA did not account for a large fraction in NK; thus, we concluded that soil emissions were not the primary source of national-scale increases of NO_2 in NK. Additionally, the negative trends of CO VCDs imply that biomass burning was not a significant NO_2 source either (see Figs. 2f, 3c, and S6c).

Kim and Kim (2019) estimated that in NK, from 2000 to 2008, industrial activities, transportation, and power generation contributed to NO_x emissions by 41.7 %, 38.4 %, and 12.7 %, respectively. Therefore, as the candidate variables to explain the increasing NO_2 patterns, we selected the 'index of all industrial production,' 'number of registered motor vehicles,' and 'electrical energy supply via thermal power generation' from the statistical indicators generated by the SK's government (Statistics Korea, 2018) (Fig. 3a). Since these statistics were derived at the national scale, only the NO_2 TVCDs averaged over the entirety of NK were analyzed here. Fig. 3a shows that thermal power generation fluctuated during the study period, and its changing patterns appeared weakly associated with the observed NO_2 TVCD variability. The number of vehicles registered in NK increased, but the trend (1.3 % yr^{-1}) was insufficient to account for the NO_2 TVCD increases alone. Conversely, the statistics reported an increase in industrial production in NK, even though coal-fired PES in NK decreased during the study period (Statistics Korea, 2018, 2019). This report implies the possibility of growth in coal-independent industrial activities and/or the transition of coal usage from other sectors into industries requiring a reduced coal supply. However, investigating which of the two scenarios applies to NK was beyond the scope of the present study. Overall, we deduced that NK's changes in industrial production could be responsible for the increasing NO_2 concentrations. This finding is consistent with a previous study that estimated that domestic NO_x emissions in NK increased by 6 % yr^{-1} from 2007 to 2011 (Mijling et al., 2013). On urban scales, NO_2 TVCDs in industrial cities such as Pyongyang, Nampo, and Pukchang increased more rapidly than the average over the entire NK territory (Fig. 2d), supporting that industrial activities are important factors accounting for the increasing NO_2 trends in NK.

Since coal combustion is the major emission source of SO_2, 'primary energy supply by coal' was selected as the lone explanatory variable of SO_2 pollution changes. The correlation coefficient between changes in the coal-fired PES and the SO_2 VCDs was 0.74 (Fig. 3b). The same explanatory variable was used to assess CO change, revealing a notably lower correlation coefficient (0.53) (Fig. 3c). As mentioned, the slighter decrease in CO VCD compared to SO_2 VCD can either be attributed to the influence of residential biomass burning or the longer lifetime of CO.

As briefly mentioned while interpreting positive NO_2 trends, transboundary pollution could contribute to the changes in NK's pollutant amounts. We attempted to remove the dependence of NK's pollution on long-range transport by applying the same correction method to each pollutant (see Supplementary data). It is worth noting that the VCDs preserved the signs of their linear trends in every region of interest in NK after correction, without decreasing patterns flipped to increasing or vice versa (See Figs. 2 and S8). On a national scale, the relative change rates of SO_2 and CO VCDs only reduced by 0.9 and 0.1 % yr^{-1}, respectively, and the NO_2 trend showed the same rate after correction. Post-correction VCDs of each pollutant showed the strongest association with the same explanatory variable as before correction, only with slightly changed correlation coefficients for SO_2 and CO (Fig. S8). These analyses with the transport-corrected VCDs support our findings that the domestic factors contributed to NK's pollution changes.

3.2. Changes in AOD and $PM_{2.5}$ concentration from March 2011 to December 2018

The average AOD over NK from March 2011 to December 2018 was 0.26 $\pm$ 0.11, notably similar to that over SK for the same period (0.28 $\pm$ 0.12) (Table 1). By normalizing the annual mean AOD with the PES, we found that NK experienced an average of 24.3 times larger AOD per unit energy supply than SK over the analysis period.

Fig. 4 shows the biennial means of AODs observed from GOCI during 2011–2018. Similar to VCDs of the gaseous pollutants, high AOD values appeared over the western parts of NK (particularly in the four cities analyzed), implying that aerosol pollution was associated with long-range transport and anthropogenic activities (especially coal combustion). Meanwhile, decreasing AODs over the analysis period were observed on a national scale.

To further investigate AOD, annual mean values were analyzed for Pyongyang, Nampo, Pukchang, Munchon, and at the national scale (Fig. 5a). Nampo maintained the highest AOD values, likely resulting from the large population, industrial activities, biofuel combustion, and transboundary transport. Notably, all the regions of interest showed negative AOD trends (Fig. 5a; Table 1). A relative linear decrease at the national scale was –4.8 $\pm$ 1.0 % yr^{-1}, and those from the selected cities ranged between –5.9 % yr^{-1} to –3.4 % yr^{-1}.

We found significant correlation coefficients between deseasonalized monthly AOD time series of the Yellow Sea and most grid pixels in NK (~81 %) from 2011 to 2018, with a national average of 0.44 (Fig. S11a). The correlation coefficients were higher in the western parts of NK, indicating a stronger influence of transboundary pollution. For example, Pyongyang showed a correlation coefficient of 0.55. Slope values derived from linear regression between the Yellow Sea and NK time series were also higher in the western parts, supporting that those regions were more sensitive to transboundary pollution (Fig. S11b). There

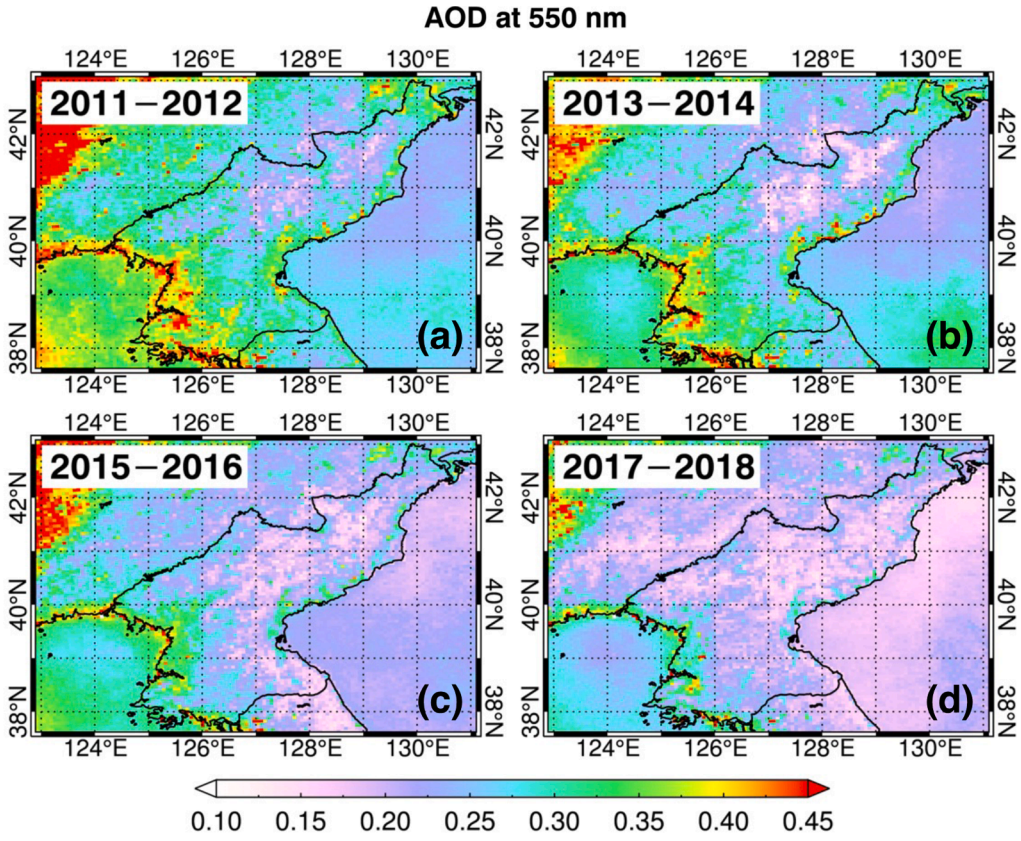

Fig. 4. Biennial means of AOD values observed at 550 nm from GOCI during 2011–2018.

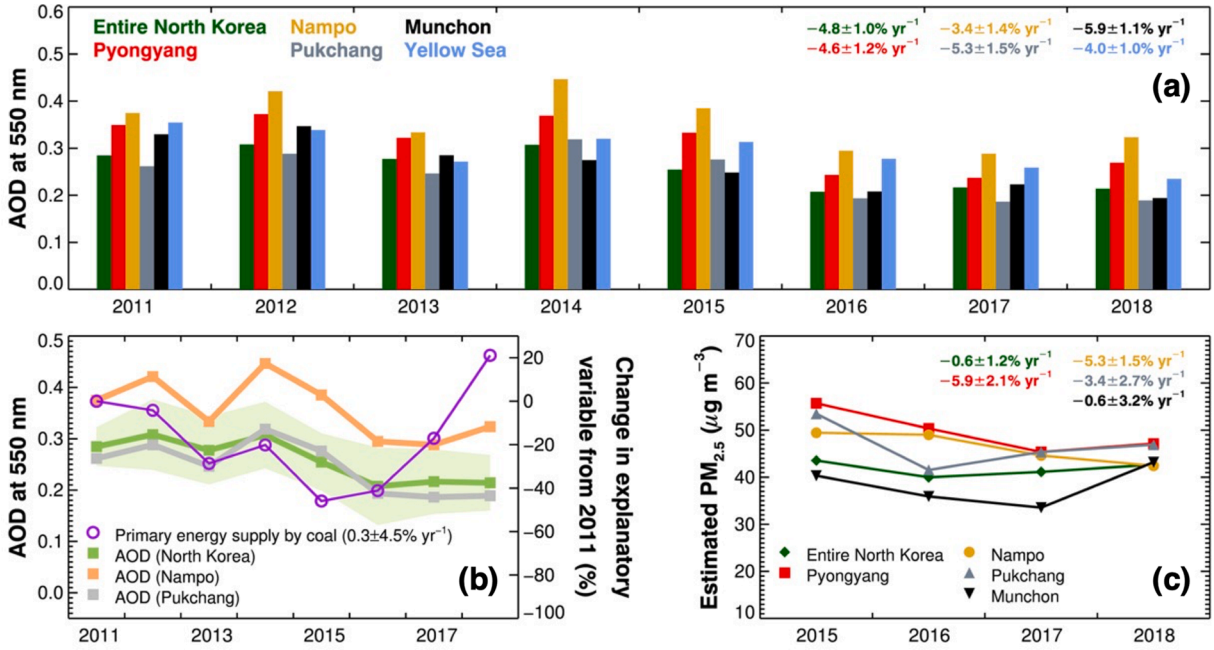

Fig. 5. Interannual changes in AOD and $PM_{2.5}$ concentrations. (a) Annual mean AODs, with inset values depicting relative trends for each region of interest; (b) AODs for entire North Korea, Nampo, and Pukchang, where green shading indicates standard deviations across the entirety of North Korea. The change in the primary explanatory variable (i.e., primary energy supply by coal) is also presented. (c) Annnual mean $PM_{2.5}$ concentrations, with inset values depicting relative trends for each region of interest. (For interpretation of the references to color in this figure legend, the reader is referred to the web version of this article.)

was a longitudinal gradient in NK's 2011–2018 mean AOD field between 124°E and 129°E with higher values in the west. We found that correcting the influence of transboundary pollution makes this gradient weaker and AODs lower (Fig. S11d). The differences between the meridional averages of pre- and post-correction AODs in NK showed a maximum of 0.086 (27.7 %) at 125.25°E and decreased eastwards up to

128.75°E, being evidence of a higher level of transboundary pollution in the western parts. Overall, urban-scale enhancements were preserved in the western parts of the transport-corrected AOD fields but with a weakened national-scale longitudinal gradient (Fig. S11c).

We estimated that transported amounts of aerosols were reduced by time, implying that the observed negative AOD trends in NK partly occurred due to a decline in transboundary aerosol pollution (Table S1). Indeed, the change rates of AODs appeared to be slower after correcting the transport influence (see Figs. 5a and S12a). Consistent with the gaseous pollutants, however, the post-correction AODs preserved the signs of trends, showing decreasing patterns in every region of interest in NK (Fig. S12a). The negative trends of post-correction AODs support the contributions of domestic factors to the decreasing AODs in NK.

To identify possible explanatory variables, we used the statistical indicators of NK generated by the SK's government (Statistics Korea, 2018, 2019), similarly to the gaseous pollutants. As with SO_2 and CO, we deduced that the 'primary energy supply by coal' was the most influential in describing the decreasing AOD trends. Fig. 5b shows the temporal changes in the coal-fired energy supply and AOD in NK from 2011 to 2018. Notably, the changing patterns of AODs in Nampo and Pukchang reflected the coal-fired PES variations (Fig. 5b), and consistent features were also found in transport-corrected AODs (Fig. S12b). This is reasonable as the air quality in these two industrial cities could heavily depend on local variations in coal consumption. Biofuel combustion is another potential factor substantially influencing AOD values (Kim et al., 2019); however, the quantification of biofuel consumption is marked by substantial uncertainty.

Estimating aerosol mass concentrations assists in intuitive assessments of aerosol amounts. GOCI estimates indicated that annual mean $PM_{2.5}$ concentrations over NK from 2015 to 2018 were 43.5, 40.0, 41.1, and 42.7 μg m^{-3} (Fig. 5c). The highest $PM_{2.5}$ concentrations appeared in Pyongyang, with corresponding annual estimates of 55.7, 50.4, 45.4, and 47.2 μg m^{-3}, respectively (Fig. 5c). These values may be accompanied by uncertainty since no ground-based measurement data were available in NK for input into the RF algorithm; however, the estimates agreed well with the mean population exposure to $PM_{2.5}$ provided by the OECD (48.0, 43.5, 43.5, and 45.1 μg m^{-3} over the entirety of NK, and 55.4, 50.5, 49.7, and 52.3 μg m^{-3} for Pyongyang from 2015 to 2018, respectively) (OECD, 2020). Similar to the findings reported by the OECD, the estimates here showed declining trends (Fig. 5c). Accordingly, the decrease in $PM_{2.5}$ concentrations was presumably driven by a reduction in coal-fired PES and a decline in transboundary aerosol pollution.

Average $PM_{2.5}$ concentrations estimated across NK (41.8 ± 12.0 μg m^{-3}) and Pyongyang (49.6 ± 13.7 μg m^{-3}) from 2015 to 2018 were both substantially higher than those of SK (27.5 ± 5.3 μg m^{-3}) and Seoul (25.5 ± 6.6 μg m^{-3}); this is consistent with previous studies reporting larger $PM_{2.5}$ emissions over NK than those over SK (Bae et al., 2018, Kim and Kim, 2019). Coal-burning and biofuel combustion are likely the major contributors to the elevated $PM_{2.5}$ concentrations in NK.

3.3. Discussion

Dividing NK's pollutant amounts by those of SK provides a useful perspective to understand NK's air quality better. Let the ratio of NK to SK be an indicator of the pollution level. The first and second highest levels were found for CO and aerosols, whose amounts in NK were larger or close to those in SK. Since they have long lifetimes in the atmosphere, their high concentrations partly resulted from long-range transport. However, considering the common emission sources of CO and aerosols, their high pollution levels also imply substantial biofuel consumption in NK, aligned with findings from previous studies. The third highest pollution level was found for SO_2, indicating 81 % of the concentrations in SK during 2005–2018. Aside from the contribution of long-range transport, the high SO_2 pollution suggests insufficient desulfurization of fuels and flue gases from the enormous coal burning in NK, although the coal-fired energy supply showed a decreasing trend. Lastly, NO_2 concentrations were as low as 31 % of those in SK on average from 2005 to 2018. However, it is worth noting that NO_2 is the only species showing positive trends. The positive NO_2 trends imply that NK increased industrial activities to combat the declining economy under decreasing energy supply conditions.

4. Conclusions

All pollutants of interest in this study showed decreasing trends except NO_2 in NK, and the most probable cause is the decline of the coal-fired energy supply. The signs of linear trends were even preserved after correcting the transboundary pollution effects. However, it is noticeable that NK still experienced significantly larger amounts of air pollutants per energy supply compared to SK from 2005 to 2018, even with the prevailing negative trends. This finding suggests low removal efficiencies and high emission coefficients in NK. Reduction of biofuel combustion seems necessary to lower CO and aerosol concentrations, and flue gas control is an essential measure to reduce SO_2 pollution.

International cooperation would be beneficial in emissions control in NK. Indeed, NK has participated in international projects as well as enacted domestic laws and policies to protect the environment (UNEP, 2012). Yeo and Kim (2018) comprehensively summarized the direction of NK's policy regarding environmental protection. In particular, NK has been actively involved in the Clean Development Mechanism (CDM) (UNFCCC, 2022), hosting projects including hydropower generation and methane emission control (NCCE, 2012). It would be most desirable to assist emission mitigation through the forms of international cooperation favored by the NK's government.

Continuous satellite data accumulation and frequent trend analysis updates are essential to link NK's air pollution with anthropogenic activities. The year 2020 would be particularly of interest in future studies since lockdown measures were globally implemented due to the spread of Coronavirus disease 2019 (COVID-19) in that year. We found that applying the same analysis method to the period 2005–2020 resulted in a linear NO_2 trend of + 2.5 % yr^{-1} (Fig. S13a), which is 2.1 % yr^{-1} lower than that from 2005–2018 (Fig. 3a), contributed by the changes in 2019 and 2020. Meanwhile, the SO_2 and CO trends showed small differences of only a few tenths of a percent or less between 2005–2018 and 2005–2020 (Figs. 3b, 3c, S13b, and S13c). Since mixed factors likely affected the decline of NK's national average NO_2 TVCDs in 2020, detailed analyses need to be conducted in the future to assess the impact of the COVID-19 lockdown on NK's air quality.

As advanced satellite instruments have continuously been developed, more precise assessments will be possible in the future. For example, the Tropospheric Monitoring Instrument (TROPOMI) (Veefkind et al., 2012) launched in 2017 is now compiling long-term VCDs of NO_2, SO_2, and CO with a higher spatial resolution than OMI. Furthermore, the Geostationary Environment Monitoring Spectrometer (GEMS) launched in 2020 has enabled the first space-borne diurnal observations of NO_2 and SO_2 VCDs over Asia (Kim et al., 2020). Such observations will contribute significantly to expanding the understanding of NK's air quality and its interactions with that in other countries in East Asia, including SK and China.

CRediT authorship contribution statement

Heesung Chong: Conceptualization, Methodology, Investigation, Writing – original draft. **Seoyoung Lee:** Conceptualization, Methodology, Investigation, Data curation. **Yeseul Cho:** Data curation, Methodology, Investigation. **Jhoon Kim:** Conceptualization, Investigation, Supervision, Resources, Funding acquisition, Writing – review & editing. **Ja-Ho Koo:** Conceptualization, Project administration, Writing – review & editing. **Yong Pyo Kim:** Conceptualization, Investigation, Methodology, Writing – review & editing. **Younha Kim:** Data curation, Methodology, Writing – review & editing. **Jung-Hun Woo:**

Conceptualization, Data curation, Writing – review & editing. **Dha Hyun Ahn:** Investigation, Methodology, Writing – review & editing.

Declaration of Competing Interest

The authors declare that they have no known competing financial interests or personal relationships that could have appeared to influence the work reported in this paper.

Data availability

Data will be made available on request.

Acknowledgements

The authors would like to acknowledge the support by Samsung Advanced Institute of Technology. This work was also supported by the Korea Ministry of Environment (MOE) under the Public Technology Program based on Environmental Policy (2017000160001). Additionally, this work was supported by Korea Environment Industry & Technology Institute (KEITI) through Climate Change R&D Project for New Climate Regime, funded by Korea Ministry of Environment (MOD) (2022003560007). The authors acknowledge the free use of the OMNO2, OMSO2, MOP02J_8, ERA5, GMTED, and GWPv4 datasets. The authors also acknowledge the free use of $PM_{2.5}$ measurements from Airkorea, the China National Urban Air Quality Real-time Publishing Platform, the Ministry of the Environment of Japan, and AEROS. GOCI data were provided by the Korea Institute of Ocean Science and Technology (KIOST). The authors acknowledge the free use of the physical oversampling algorithm developed by Kang Sun (https://github.com/Kang-Sun-CfA/Oversampling_matlab). The authors would like to thank Sara-Eva Mártinez-Alonso and David P. Edwards for their assistance with the MOPITT CO data interpretation. The authors also would like to thank Daniel Jacob and Min Ju Yeo for the fruitful discussion.

Appendix A. Supplementary material

Supplementary data to this article can be found online at https://doi.org/10.1016/j.envint.2022.107708.

References

Apte, J.S., Marshall, J.D., Cohen, A.J., Brauer, M., 2015. Addressing global mortality from ambient $PM_{2.5}$. Environ. Sci. Technol. 49, 8057–8066. https://doi.org/10.1021/acs.est.5b01236.

Bae, M., Kim, H.C., Kim, B.-U., Kim, S., 2018. $PM_{2.5}$ simulations for the Seoul Metropolitan area: (V) Estimation of North Korean emission contribution. J. Korean Soc. Atmos. Environ. 34, 294–305. https://doi.org/10.5572/KOSAE.2018.34.2.294.

Bhardwaj, P., Ki, S.J., Kim, Y.H., Woo, J.H., Song, C.K., Park, S.Y., Song, C.H., 2019. Recent changes of trans-boundary air pollution over the Yellow Sea: implications for future air quality in South Korea. Environ. Pollut. 247, 401–409. https://doi.org/10.1016/j.envpol.2019.01.048.

Breiman, L., 2001. Random forests. Mach. Learn. 45, 5–32. https://doi.org/10.1023/A:1010933404324.

Cai, K., Li, S., Lai, J., Xia, Y., Wang, Y., Hu, X., Li, A., 2022. Evaluation of TROPOMI and OMI tropospheric NO_2 products using measurements from MAX-DOAS and state-controlled stations in the Jiangsu province of China. Atmosphere 13, 886. https://doi.org/10.3390/atmos13060886.

Chawla, N.V., Bowyer, K.W., Hall, L.O., Kegelmeyer, W.P., 2002. SMOTE: Synthetic Minority Over-sampling Technique. J. Artif. Intell. Res. 16, 321–357. https://doi.org/10.1613/jair.953.

Cheng, S., Ma, J., Cheng, W., Yan, P., Zhou, H., Zhou, L., Yang, P., 2019. Tropospheric NO_2 vertical column densities retrieved from ground-based MAX-DOAS measurements at Shangdianzi regional atmospheric background station in China. J. Environ. Sci. 80, 186–196. https://doi.org/10.1016/j.jes.2018.12.012.

Choi, M., Kim, J., Lee, J., Kim, M., Park, Y.-J., Jeong, U., Kim, W., Hong, H., Holben, B., Eck, T.F., Song, C.H., Lim, J.-H., Song, C.-K., 2016. GOCI Yonsei Aerosol Retrieval (YAER) algorithm and validation during the DRAGON-NE Asia 2012 campaign. Atmos. Meas. Tech. 9, 1377–1398. https://doi.org/10.5194/amt-9-1377-2016.

Choi, M., Kim, J., Lee, J., Kim, M., Park, Y.-J., Holben, B., Eck, T.F., Li, Z., Song, C.H., 2018. GOCI Yonsei aerosol retrieval version 2 products: An improved algorithm and error analysis with uncertainty estimation from 5-year validation over East Asia. Atmos. Meas. Tech. 11, 385–408. https://doi.org/10.5194/amt-11-385-2018.

Choi, M., Lim, H., Kim, J., Lee, S., Eck, T.F., Holben, B.N., Garay, M.J., Hyer, E.J., Saide, P.E., Liu, H., 2019. Validation, comparison, and integration of GOCI, AHI, MODIS, MISR, and VIIRS aerosol optical depth over East Asia during the 2016 KORUS-AQ campaign. Atmos. Meas. Tech. 12, 1–31. https://doi.org/10.5194/amt-12-4619-2019.

Choi, J.-K., Park, Y.J., Ahn, J.H., Lim, H.-S., Eom, J., Ryu, J.-H., 2012. GOCI, the world's first geostationary ocean color observation satellite, for the monitoring of temporal variability in coastal water turbidity. J. Geophys. Res. 117 https://doi.org/10.1029/2012JC008046.

Choi, J., Park, R.J., Lee, H.-M., Lee, S., Jo, D.S., Jeong, J.I., Henze, D.K., Woo, J.-H., Ban, S.-J., Lee, M.-D., Lim, C.-S., Park, M.-K., Shin, H.J., Cho, S., Peterson, D., Song, C.-K., 2019. Impacts of local vs. trans-boundary emissions from different sectors on $PM_{2.5}$ exposure in South Korea during the KORUS-AQ campaign. Atmos. Environ. 203, 196–205. https://doi.org/10.1016/j.atmosenv.2019.02.008.

Conrad, R., 1996. Metabolism of nitric oxide in soil and soil microorganisms and regulation of flux into the atmosphere. Microbiol. Atmos. Trace Gases 60, 167–203. https://doi.org/10.1007/978-3-642-61096-7_11.

Deeter, M., Francis, G., Gille, J., Mao, D., Martínez-Alonso, S., Worden, H., Ziskin, D., Drummond, J., Commane, R., Diskin, G., McKain, K., 2022. The MOPITT version 9 CO product: sampling enhancements and validation. Atmos. Meas. Tech. 15, 2325–2344. https://doi.org/10.5194/amt-15-2325-2022.

Dormels, R., 2014. North Korea's Cities: Industrial Facilities, Internal Structure and Typification, Jimoondang.

Edwards, D.P., Emmons, L.K., Hauglustaine, D.A., Chu, D.A., Gille, J.C., Kaufman, Y.J., Pétron, G., Yurganov, L.N., Giglio, L., Deeter, M.N., Yudin, V., Ziskin, D.C., Warner, J., Lamarque, J.-F., Francis, G.L., Ho, S.P., Mao, D., Chen, J., Grechko, E.I., Drummond, J.R., 2004. Observations of carbon monoxide and aerosols from the Terra satellite: Northern Hemisphere variability. J. Geophys. Res. 109, 1–17. https://doi.org/10.1029/2004JD004727.

Feng, X., Li, Q., Zhu, Y., Hou, J., Jin, L., Wang, J., 2015. Artificial neural networks forecasting of $PM_{2.5}$ pollution using air mass trajectory based geographic model and wavelet transformation. Atmos. Environ. 107, 118–128. https://doi.org/10.1016/j.atmosenv.2015.02.030.

Fioletov, V.E., McLinden, C.A., Krotkov, N., Moran, M.D., Yang, K., 2011. Estimation of SO_2 emissions using OMI retrievals. Geophys. Res. Lett. 38, 1–5. https://doi.org/10.1029/2011GL049402.

Fioletov, V.E., McLinden, C.A., Krotkov, N., Li, C., Joiner, J., Theys, N., Carn, S., Moran, M.D., 2016. A global catalogue of large SO_2 sources and emissions derived from the Ozone Monitoring Instrument. Atmos. Chem. Phys. 16, 11497–11519. https://doi.org/10.5194/acp-16-11497-2016.

Han, K.M., 2020. Temporal analysis of OMI-observed tropospheric NO_2 columns over East Asia during 2006–2015. Atmosphere 10, 658. https://doi.org/10.3390/atmos10110658.

Han, K.M., Lee, C.K., Lee, J., Kim, J., Song, C.H., 2011. A comparison study between model-predicted and OMI-retrieved tropospheric NO_2 columns over the Korean peninsula. Atmos. Environ. 45, 2962–2971. https://doi.org/10.1016/j.atmosenv.2010.10.016.

Han, K.M., Kim, H.S., Song, C.H., 2020. An estimation of top-down NO_x emissions from OMI sensor over East Asia. Remote Sens. 12, 2004. https://doi.org/10.3390/rs12122004.

Hersbach, H., Bell, B., Berrisford, P., Hirahara, S., Horányi, A., Muñoz-Sabater, J., Nicolas, J., Peubey, C., Radu, R., Schepers, D., Simmons, A., Soci, C., Abdalla, S., Abellan, X., Balsamo, G., Bechtold, P., Biavati, G., Bidlot, J., Bonavita, M., De Chiara, G., Dahlgren, P., Dee, D., Diamantakis, M., Dragani, R., Flemming, J., Forbes, R., Fuentes, M., Geer, A., Haimberger, L., Healy, S., Hogan, R.J., Hólm, E., Janisková, M., Keeley, S., Laloyaux, P., Lopez, P., Lupu, C., Radnoti, G., de Rosnay, P., Rozum, I., Vamborg, F., Villaume, S., Thépaut, J.-N., 2020. The ERA5 global reanalysis. Q. J. R. Meteorol. Soc. 146, 1999–2049. https://doi.org/10.1002/qj.3803.

Jung, J., Choi, Y., Souri, A.H., Mousavinezhad, S., Sayeed, A., Lee, K., 2022. The impact of springtime-transported air pollutants on local air quality with satellite-constrained NO_x emission adjustments over East Asia. J. Geophys. Res. 127 https://doi.org/10.1029/2021JD035251 e2021JD035251.

Kim, J., Jeong, U., Ahn, M.-H., Kim, J.H., Park, R.J., Lee, H., Song, C.H., Choi, Y.-S., Lee, K.-H., Yoo, J.-M., Jeong, M.-J., Park, S.K., Lee, K.-M., Song, C.-K., Kim, S.-W., Kim, Y.-J., Kim, S.-W., Kim, M., Go, S., Liu, X., Chance, K., Chan Miller, C., Al-Saadi, J., Veihelmann, B., Bhartia, P.K., Torres, O., González Abad, G., Haffner, D.P., Ko, D.H., Lee, S.H., Woo, J.-H., Chong, H., Park, S.S., Nicks, D., Choi, W.J., Moon, K.-J., Cho, A., Yoon, J., Kim, S.-K., Hong, H., Lee, K., Lee, H., Lee, S., Choi, M., Veefkind, P., Levelt, P., Edwards, D.P., Kang, M., Eo, M., Bak, J., Baek, K., Kwon, H.-A., Yang, J., Park, J., Han, K.M., Kim, B.-R., Shin, H.-W., Choi, H., Lee, E., Chong, J., Cha, Y., Koo, J.-H., Irie, H., Hayashida, S., Kasai, Y., Kanaya, Y., Liu, C., Lin, J., Crawford, J.H., Carmichael, G.R., Newchurch, M.J., Lefer, B.L., Herman, J.R., Swap, R.J., Lau, A.K.H., Kurosu, T.P., Jaross, G., Ahlers, B., Dobber, M., McElroy, T., Choi, Y., 2020. New era of air quality monitoring from space: Geostationary Environment Monitoring Spectrometer (GEMS). Bull. Am. Meteorol. Soc. 101, E1–E22. https://doi.org/10.1175/BAMS-D-18-0013.1.

Kim, N.K., Kim, Y.P., Morino, Y., Kurokawa, J., Ohara, T., 2014. Verification of NO_x emission inventories over North Korea. Environ. Pollut. 195, 236–244. https://doi.org/10.1016/j.envpol.2014.06.034.

Kim, I.S., Kim, Y.P., 2019. Characteristics of energy usage and emissions of air pollutants in North Korea. J. Korean Soc. Atmos. Environ. 35, 125–137. https://doi.org/10.5572/KOSAE.2019.35.1.125.

Kim, I.S., Lee, J.Y., Kim, Y.P., 2011. Energy usage and emissions of air pollutants in North Korea. J. Korean Soc. Atmos. Environ. 27, 303–312. https://doi.org/10.5572/KOSAE.2011.27.3.303.

Kim, I.S., Lee, J.Y., Kim, Y.P., 2013. Impact of polycyclic aromatic hydrocarbon (PAH) emissions from North Korea to the air quality in the Seoul Metropolitan Area, South Korea. Atmos. Environ. 70, 159–165. https://doi.org/10.1016/j.atmosenv.2012.12.040.

Kim, I.S., Wee, D., Kim, Y.P., Lee, J.Y., 2016. Development and application of three-dimensional potential source contribution function (3D-PSCF). Environ. Sci. Pollut. Res. Int. 23, 16946–16954. https://doi.org/10.1007/s11356-016-6787-x.

Kim, I.S., Lee, J.Y., Wee, D., Kim, Y.P., 2019. Estimation of the contribution of biomass fuel burning activities in North Korea to the air quality in Seoul, South Korea: Application of the 3D-PSCF method. Atmos. Res. 230, 104628 https://doi.org/10.1016/j.atmosres.2019.104628.

IEA, 2022. World Energy Balances. https://www.iea.org/countries/korea-democratic-peoples-republic-of (accessed 7 August 2022).

Mijling, B., van der A, R.J., Zhang, Q., 2013. Regional nitrogen oxides emission trends in East Asia observed from space. Atmos. Chem. Phys. 13, 12003–12012. https://doi.org/10.5194/acp-13-12003-2013.

Krotkov, N.A., Lamsal, L.N., Marchenko, S.V., Bucsela, E.J., Swartz, W.H., Joiner, J., the OMI core team, 2019a. OMI/Aura Nitrogen Dioxide (NO_2) Total and Tropospheric Column 1-Orbit L2 Swath 13x24 km V003, Goddard Earth Sciences Data and Information Services Center, Greenbelt, MD, USA. https://doi.org/10.5067/Aura/OMI/DATA2017.

Krotkov, N.A., Lamsal, L.N., Marchenko, S.V., Swartz, W.H., 2019b. OMNO2 README Document Data Product Version 4.0. https://aura.gesdisc.eosdis.nasa.gov/data/Aura_OMI_Level2/OMNO2.003/doc/README.OMNO2.pdf (accessed 7 August 2022).

Krotkov, N.A., Li, C., Leonard, P.J.T., 2020. README Document for OMSO2: Aura/OMI Sulfur Dioxide Level 2 Product. https://aura.gesdisc.eosdis.nasa.gov/data/Aura_OMI_Level2/OMSO2.003/doc/OMSO2Readme_V2.pdf (accessed 7 August 2022).

Krotkov, N.A., McLinden, C.A., Li, C., Lamsal, L.N., Celarier, E.A., Marchenko, S.V., Swartz, W.H., Bucsela, E.J., Joiner, J., Duncan, B.N., Boersma, K.F., Veefkind, J.P., Levelt, P.F., Fioletov, V.E., Dickerson, R.R., He, H., Lu, Z., Streets, D.G., 2016. Aura OMI observations of regional SO_2 and NO_2 pollution changes from 2005 to 2015. Atmos. Chem. Phys. 16, 4605–4629. https://doi.org/10.5194/acp-16-4605-2016.

Kurosu, T.P., Celarier, E.A., 2010. OMPIXCOR README FILE. https://aura.gesdisc.eosdis.nasa.gov/data/Aura_OMI_Level2/OMPIXCOR.003/doc/README.OMPIXCOR.pdf (accessed 7 August 2022).

Lamsal, L.N., Krotkov, N.A., Vasilkov, A., Marchenko, S., Qin, W., Yang, E.-S., Fasnacht, Z., Joiner, J., Choi, S., Haffner, D., Swartz, W.H., Fisher, B., Bucsela, E., 2021. Ozone Monitoring Instrument (OMI) Aura nitrogen dioxide standard product version 4.0 with improved surface and cloud treatments. Atmos. Meas. Tech. 14, 455–479. https://doi.org/10.5194/amt-14-455-2021.

Lee, J., Kim, J., Song, C.H., Ryu, J.-H., Ahn, Y.-H., Song, C.K., 2010. Algorithm for retrieval of aerosol optical properties over the ocean from the Geostationary Ocean Color Imager. Remote Sens. Environ. 114, 1077–1088. https://doi.org/10.1016/j.rse.2009.12.021.

Lee, H.-J., Kim, S.-W., Brioude, J., Cooper, O.R., Frost, G.J., Kim, C.-H., Park, R.J., Trainer, M., Woo, J.-H., 2014. Transport of NO_x in East Asia identified by satellite and in situ measurements and Lagrangian particle dispersion model simulation. J. Geophys. Res. Atmos. 16, 2574–2596. https://doi.org/10.1002/2013JD021185.

Lee, S., Kim, J., Choi, M., Hong, J., Lim, H., Eck, T.F., Holben, B.N., Ahn, J.-Y., Kim, J., Koo, J.-H., 2019. Analysis of long-range transboundary transport (LRTT) effect on Korean aerosol pollution during the KORUS-AQ campaign. Atmos. Environ. 204, 53–67. https://doi.org/10.1016/j.atmosenv.2019.02.020.

Lee, S., Kim, M., Kim, S.-Y., Lee, D.-W., Lee, H., Kim, J., Le, S., Liu, Y., 2021. Assessment of long-range transboundary aerosols in Seoul, South Korea from Geostationary Ocean Color Imager (GOCI) and ground-based observations. Environ. Pollut. 269, 115924 https://doi.org/10.1016/j.envpol.2020.115924.

Levelt, P.F., van den Oord, G.H.J., Dobber, M.R., Malkki, A., Visser, H., de Vries, J., Stammes, P., Lundell, J.O.V., Saari, H., 2006. The Ozone Monitoring Instrument. IEEE Trans. Geosci. Remote Sens. 44, 1093–1101. https://doi.org/10.1109/TGRS.2006.872333.

Li, C., Krotkov, N.A., Leonard, P.J.T., Carn, S., Joiner, J., Spurr, R.J.D., Vasilkov, A., 2020a. Version 2 ozone monitoring instrument SO_2 product (OMSO2 V2): new anthropogenic SO_2 vertical column density dataset. Atmos. Meas. Tech. 13, 6175–6191. https://doi.org/10.5194/amt-13-6175-2020.

Li, C., Krotkov, N.A., Leonard, P., Joiner, J., 2020b. OMI/Aura Sulphur Dioxide (SO_2) Total Column 1-Orbit L2 Swath 13x24 km V003. Goddard Earth Sciences Data and Information Services Center, Greenbelt, MD, USA. https://doi.org/10.5067/Aura/OMI/DATA2022.

MOPITT Algorithm Development Team, 2018. MOPITT (Measurements of Pollution in the Troposphere) Version 8 Product User's Guide. https://www2.acom.ucar.edu/sites/default/files/documents/v8_users_guide_201812.pdf (accessed 7 August 2022).

NASA/LARC/SD/ASDC, 2000. MOPITT Derived CO (Near and Thermal Infrared Radiances) V008, NASA Langley Atmospheric Science Data Center DAAC. https://doi.org/10.5067/TERRA/MOPITT/MOP02J_L2.008 (accessed 7 August 2022).

NCCE, 2012. DPR Korea's Second National Communication on Climate Change, Pyongyang. https://unfccc.int/sites/default/files/resource/prknc2.pdf (accessed 20 November 2022).

OECD, 2020, Exposure to $PM_{2.5}$ in countries and regions, OECD Statistics. https://stats.oecd.org/Index.aspx?DataSetCode=EXP_PM2_5 (accessed 7 August 2022).

Park, S., Shin, M., Im, J., Song, C.-K., Choi, M., Kim, J., Lee, S., Park, R., Kim, J., Lee, D.-W., Kim, S.-K., 2019. Estimation of ground-level particulate matter concentrations through the synergistic use of satellite observations and process-based models over South Korea. Atmos. Chem. Phys. 19, 1097–1113. https://doi.org/10.5194/acp-19-1097-2019.

Pommier, M., McLinden, C.A., Deeter, M., 2013. Relative changes in CO emissions over megacities based on observations from space. Geophys. Res. Lett. 40, 3766–3771. https://doi.org/10.1002/grl.50704.

Qu, Z., Henze, D.K., Worden, H.M., Jiang, Z., Gaubert, B., Theys, N., Wang, W., 2022. Sector-based top-down estimates of NO_x, SO_2, and CO emissions in East Asia. Geophys. Res. Lett. 49 https://doi.org/10.1029/2021GL096009 e2021GL096009.

Ridley, B.A., Dye, J.E., Walega, J.G., Zheng, J., Grahek, F.E., Rison, W., 1996. On the production of active nitrogen by thunderstorms over New Mexico. J. Geophys. Res. Atmos. 101, 20985–21005. https://doi.org/10.1029/96JD01706.

Rodríguez, J.D., Pérez, A., Lozano, J.A., 2010. Sensitivity analysis of k-fold cross validation in prediction error estimation. IEEE Trans. Pattern Anal. Mach. Intell. 32, 569–575. https://doi.org/10.1109/TPAMI.2009.187.

Schenkeveld, V.M.E., Jaross, G., Marchenko, S., Haffner, D., Kleipool, Q.L., Rozemeijer, N.C., Veefkind, J.P., Levelt, P.F., 2017. In-flight performance of the Ozone Monitoring Instrument. Atmos. Meas. Tech. 10, 1957–1986. https://doi.org/10.5194/amt-10-1957-2017.

Si, Y., Wang, H., Cai, K., Chen, L., Zhou, Z., Li, S., 2019. Long-term (2006–2015) variations and relations of multiple atmospheric pollutants based on multi-remote sensing data over the North China Plain. Environ. Pollut. 255, 113323. https://doi.org/10.1016/j.envpol.2019.113323.

Smith, S.J., van Aardenne, J., Klimont, Z., Andres, R.J., Volke, A., Delgado Arias, S., 2011. Anthropogenic sulfur dioxide emissions: 1850–2005. Atmos. Chem. Phys. 11, 1101–1116. https://doi.org/10.5194/acp-11-1101-2011.

Souri, A.H., Choi, Y., Jeon, W., Woo, J.-H., Zhang, Q., Kurokawa, J.-I., 2017. Remote sensing evidence of decadal changes in major tropospheric ozone precursors over East Asia. J. Geophys. Res. Atmos. 122, 2474–2492. https://doi.org/10.1002/2016JD025663.

Statistics Korea, 2018. Major Statistics Indicators of North Korea. https://kosis.kr/upsHtml/upload/Magazine/NEW/IF/bukhanY18.pdf (accessed 7 August 2022).

Statistics Korea, 2019. Major Statistics Indicators of North Korea. https://kosis.kr/upsHtml/upload/Magazine/NEW/IF/bukhanY19.pdf (accessed 7 August 2022).

Streets, D.G., Bond, T.C., Carmichael, G.R., Fernandes, S.D., Fu, Q., He, D., Klimont, Z., Nelson, S.M., Tsai, N.Y., Wang, M.Q., Woo, J.-H., Yarber, K.F., 2003. An inventory of gaseous and primary aerosol emissions in Asia in the year 2000. J. Geophys. Res. 108 https://doi.org/10.1029/2002JD003093.

Sun, K., Zhu, L., Cady-Pereira, K., Chan Miller, C., Chance, K., Clarisse, L., Coheur, P.-F., González Abad, G., Huang, G., Liu, X., Van Damme, M., Yang, K., Zondlo, M., 2018. A physics-based approach to oversample multi-satellite, multispecies observations to a common grid. Atmos. Meas. Tech. 11, 1–30. https://doi.org/10.5194/amt-11-6679-2018.

Tian, X., Xie, P., Xu, J., Li, A., Wang, Y., Qin, M., Hu, Z., 2018. Long-term observations of tropospheric NO_2, SO_2, and HCHO by MAX-DOAS in Yangtze River Delta area. China. *J. Environ. Sci.* 71, 207–221. https://doi.org/10.1016/j.jes.2018.03.006.

UNEP, 2012. Democratic People's Republic of Korea Environment and Climate Change Outlook. https://wedocs.unep.org/bitstream/handle/20.500.11822/9679/-Environment_and_Climate_Change_Outlook-2012ECCO_DPRK_2012.pdf.pdf?sequence=3&amp%3BisAllowed= (accessed 7 August 2022).

UNFCCC, 2022. Clean Development Mechanism (CDM). https://cdm.unfccc.int/ (accessed 20 November 2022).

Van Damme, M., Clarisse, L., Whitburn, S., Hadji-Lazaro, J., Hurtmans, D., Clerbaux, C., Coheur, P.-F., 2018. Industrial and agricultural ammonia point sources exposed. Nature 564, 99–103. https://doi.org/10.1038/s41586-018-0747-1.

van der A, R.J., Eskes, H.J., Boersma, K.F., van Noije, T.P.C., Van Roozendael, M., De Smedt, I., Peters, D.H.M.U., Meijer, E.W., 2008. Trends, seasonal variability and dominant NO_x source derived from a ten year record of NO_2 measured from space. *J. Geophys. Res. Atmos.* 113, 1–12. https://doi.org/10.1029/2007JD009021.

Van Vuuren, D.P., Bouwman, L.F., Smith, S.J., Dentener, F., 2011. Global projections for anthropogenic reactive nitrogen emissions to the atmosphere: An assessment of scenarios in the scientific literature. Curr. Opin. Environ. Sustain. 3, 359–369. https://doi.org/10.1016/j.cosust.2011.08.014.

Veefkind, J.P., Aben, I., McMullan, K., Förster, H., de Vries, J., Otter, G., Claas, J., Eskes, H.J., de Haan, J.F., Kleipool, Q., van Weele, M., Hasekamp, O., Hoogeveen, R., Landgraf, J., Snel, R., Tol, P., Ingmann, P., Voors, R., Kruizinga, B., Vink, R., Visser, H., Levelt, P.F., 2012. TROPOMI on the ESA Sentinel-5 Precursor: A GMES mission for global observations of the atmospheric composition for climate, air quality and ozone layer applications. Remote Sens. Environ. 120, 70–83. https://doi.org/10.1016/j.rse.2011.09.027.

Weatherhead, E.C., Reinsel, G.C., Tiao, G.C., Meng, X.-L., Choi, D., Cheang, W.-K., Keller, T., DeLuisi, J., Wuebbles, D.J., Kerr, J.B., Miller, A.J., Oltmans, S.J., Frederick, J.E., 1998. Factors affecting the detection of trends: Statistical considerations and applications to environmental data. J. Geophys. Res. 103, 17149–17161. https://doi.org/10.1029/98JD00995.

WHO, 2022. Indicator 3.9.1: mortality rate attributed to household and ambient air pollution (per 100 100 population), The Global Health Observatory. https://www.who.int/data/gho/data/indicators/indicator-details/GHO/ambient-and-household-air-pollution-attributable-death-rate-(per-100-000-population) (accessed 1 November 2022).

Wu, J.-Z., Ge, D.-D., Zhou, L.-F., Hou, L.-Y., Zhou, Y., Li, Q.-Y., 2018. Effects of particulate matter on allergic respiratory diseases. Chronic Dis. Transl. Med. 4, 95–102. https://doi.org/10.1016/j.cdtm.2018.04.001.

Yeo, M.J., Kim, Y.P., 2018. Electricity supply trend and operating statuses of coal-fired power plants in North Korea using the facility-specific data produced by North Korea: Characterization and recommendations. Air Qual. Atmos. Health 11, 979–992. https://doi.org/10.1007/s11869-018-0601-5.

Yeo, M.J., Kim, Y.P., 2019. The state of the air quality and measures for improving it in North Korea. J. Korean Soc. Atmos. Environ. 35, 318–335. https://doi.org/10.5572/KOSAE.2019.35.3.318.

Yeo, M.J., Seo, J., Kim, Y.P., 2019. Temporal and spatial characteristics of visibility in North Korea. J. Korean Soc. Atmos. Environ. 35, 726–740. https://doi.org/10.5572/KOSAE.2019.35.6.726.

Zheng, B., Chevallier, F., Ciais, P., Yin, Y., Deeter, M.N., Worden, H.M., Wang, Y., Zhang, Q., He, K., 2018. Rapid decline in carbon monoxide emissions and export from East Asia between years 2005 and 2016. Environ. Res. 13, 044007 https://doi.org/10.1088/1748-9326/aab2b3.

Zhong, Q., Huang, Y., Shen, H., Chen, Y., Chen, H., Huang, T., Zeng, E.Y., Tao, S., 2017. Global estimates of carbon monoxide emissions from 1960 to 2013. Environ. Sci. Pollut. Res. Int. 24, 864–873. https://doi.org/10.1007/s11356-016-7896-2.

Zhu, L., Jacob, D.J., Keutsch, F.N., Mickley, L.J., Scheffe, R., Strum, M., González Abad, G., Chance, K., Yang, K., Rappenglück, B., Millet, D.B., Baasandorj, M., Jaeglé, L., Shah, V., 2017. Formaldehyde (HCHO) as a hazardous air pollutant: Mapping surface air concentrations from satellite and inferring cancer risks in the United States. Environ. Sci. Technol. 51, 5650–5657. https://doi.org/10.1021/acs.est.7b01356.